J. Fluid Mech. (1980), *vol.* 97, *part* 2, *pp.* 385–404
Printed in Great Britain

Applicability of the isotropic vorticity theory to an adverse pressure gradient flow

By S. C. ARORA† AND R. S. AZAD

Department of Mechanical Engineering, The University of Manitoba, Winnipeg, Manitoba, Canada R3T 2N2

(Received 1 November 1978 and in revised form 30 July 1979)

An examination of the isotropic vorticity theory was made in an adverse pressure gradient flow based on experimental data obtained in a conical diffuser having a total divergence angle of 8° and an area ratio of 4:1 with fully-developed pipe flow at entry. The results showed that the rates and the ratio of production and dissipation of the turbulent vorticity were constant in the core region of the diffuser but increase significantly in the wall layer. The overall vorticity balance was essentially the same at all axial stations. The analysis of Batchelor & Townsend (1947) for isotropic vorticity was found to be valid in the core region of the diffuser for an order-of-magnitude higher R_λ ($200 \leqslant R_\lambda \leqslant 600$) than in grid turbulence. The magnitude of the skewness of $\partial u_1/\partial t$ was constant in the core region and comparable to that for grid turbulence. Also, this region of constant skewness extended over a larger portion of the flow cross-section compared to pipe flow. On the basis of these results, it was concluded that assumptions of isotropy in the fine structure are valid in the core region of the diffuser.

1. Introduction

The turbulent flow of real fluids is of a dissipative nature. Owing to this dissipation of turbulent energy, a continuous supply of energy from some external source is necessary to maintain the turbulence. This external source is usually the mean flow. The rate of supply of kinetic energy to the turbulence is the rate at which work is done by the mean rate of strain against the Reynolds stresses in the flow as it stretches the turbulent vortex lines. The extraction of this energy from the mean flow occurs at large scales and this gain is balanced by viscous dissipation of energy at very small scales.

The smaller eddies are exposed to the strain-rate field of the larger eddies. Because of the straining, the vorticity of the smaller eddies increases, with a consequent increase in their energy at the expense of the energy of the larger eddies. In this way, there is a flux of energy from larger to smaller eddies which subsequently undergo viscous decay. The mechanism of vortex stretching for energy transfer to smaller eddies also makes the smaller eddies lose all sense of direction and thus attain the state of isotropy, a concept introduced by G. I. Taylor in 1935. By considering the multiple-scale cumulative expansion of spectra for isotropic turbulence, Tatsumi, Kida & Mizushima (1978) have shown that the small-scale structure is essentially independent of its large-scale

† Permanent address: Structures Analysis Turbine Department, Pratt & Whitney Aircraft of Canada Ltd., Longueuil, Quebec, Canada J4K 4X9.

0022-1120/80/4409-8550 $02.00

structure. Also, the structure of these smaller eddies is similar for all turbulent flows (Batchelor 1947).

Though the supply of turbulent energy is at large scales, its dissipation is at the smallest scales. These smaller eddies also represent the turbulent vorticity field and thus characterize the flow as rotational and dissipative. Therefore, the study of the turbulent vorticity balance is essentially an attempt to understand the finer structure of turbulence which is inevitably required for better understanding of the turbulence mechanism. Furthermore, in most turbulent flow calculations, the isotropic vorticity theory is assumed and yet it has seldom been verified. The object of the present work was to study the applicability of the isotropic vorticity theory to a flow subjected to adverse pressure gradient. The study, in effect, tests the similarity of the isotropic character of smaller eddies as proposed by Batchelor (1947).

Physically, a diffuser converts mean kinetic energy into flow energy which produces a positive (adverse) pressure gradient in the direction of flow. This also increases the intensity of highly-energetic turbulent processes near the wall, which results in high turbulence intensities in the flow field. This high intensity of turbulence makes the diffuser research experimentally challenging and, furthermore, the effect of adverse pressure gradient on the structure of turbulence is desirable from the point of view of scientific knowledge and engineering application. The conical geometry of the diffuser provides an axisymmetric distribution of the mean and turbulent quantities.

The conical diffuser chosen for this study was the same as that used by Okwuobi & Azad (1973), having an 8° included angle and an area ratio of 4:1 with fully-developed pipe flow at entry. Sovran & Klomp (1967) have shown that such a diffuser possesses optimum pressure-recovery characteristics.

2. Theoretical relations

The general turbulent vorticity equation can be obtained directly from the Navier–Stokes equation [Corrsin & Kistler 1955, equation (12); Tennekes & Lumley 1972, equation (3.3.38)]. The vorticity equation for isotropic turbulence was derived by von Kármán in the form [as reported by Batchelor & Townsend 1947; also deduced by Corrsin & Kistler 1955, equation (17)]

$$3\frac{d\overline{\omega'^2}}{dt} = 2\overline{\omega_i \omega_j \frac{\partial u_i}{\partial x_j}} + 2\nu\overline{\omega_i \frac{\partial^2 \omega_i}{\partial x_j^2}}, \tag{1}$$

where $\omega_i = \epsilon_{ijk}\,\partial u_k/\partial x_j$; ω' is the r.m.s. of the fluctuating vorticity vector, u_i is the fluctuating velocity in x_i direction, t is time, and ν is the kinematic viscosity of the fluid. The first term on the right-hand side is positive and represents the rate of production of vorticity, whereas the second term on the right-hand side represents a rate of destruction of vorticity due to viscosity (viscous transport and dissipation). Since

$$2\overline{\omega_i \frac{\partial^2 \omega_i}{\partial x_j^2}} = \overline{\frac{\partial^2 \omega_i^2}{\partial x_j^2}} - 2\overline{\left(\frac{\partial \omega_i}{\partial x_j}\right)^2} \tag{2}$$

and $(\overline{\partial^2 \omega_i^2/\partial x_j^2})$ is zero in a homogeneous field, the term is essentially negative.

In a flow field, when positive extension of a vortex filament occurs, the magnitude of the local vorticity increases owing to consequent lateral contraction and angular

acceleration. Thus, in parts of the fluid where there is a positive rate of extension of the vortex filament, the magnitude of the vorticity will be high. Taylor (1938) pointed out that this production of vorticity due to random, diffusive extension of vortex lines is a fundamental process in the mechanics of turbulence and is the reason for the very high rate of dissipation of turbulence energy.

The effect of extension of the vortex lines is to tend to make the vorticity distribution 'spotty', with small regions of high vorticity; on the other hand, the effect of viscosity is strongest in regions of high vorticity, and tends to diffuse it evenly throughout the fluid (Batchelor & Townsend 1947). The vorticity equation (1) represents the balance between these effects, and a simplified form of this equation which could be used for comparison with experiment has been given by Batchelor & Townsend as

$$\frac{d\omega'^2}{dt} = \frac{7}{3\sqrt{5}}\omega'^3 S - \frac{14}{3\sqrt{5}}\omega'^3 \frac{G}{R_\lambda}, \tag{3}$$

where S is the minus skewness factor of the probability distribution of $\partial u_1/\partial x_1$ (the minus sign is introduced because the skewness is found to be negative) defined as

$$S = -\frac{\overline{(\partial u_1/\partial x_1)^3}}{[\overline{(\partial u_1/\partial x_1)^2}]^{\frac{3}{2}}}. \tag{4}$$

The contribution to $d\omega'^2/dt$ from the process of vortex extension is directly proportional to S. The factor G/R_λ is related to the decay of vorticity due to viscosity and is defined as

$$G = u_1'^2 \frac{\overline{(\partial^2 u_1/\partial x_1^2)^2}}{[\overline{(\partial u_1/\partial x_1)^2}]^2} \tag{5}$$

and

$$R_\lambda = u'_{1\lambda}/\nu, \tag{6}$$

where λ is the Taylor microscale.

Representative measures of the factors S, G and λ can be obtained by measuring time derivatives of u_1 and using Taylor's assumption of space–time equivalence. Thus

$$S = \frac{\overline{(\partial u_1/\partial t)^3}}{[\overline{(\partial u_1/\partial t)^2}]^{\frac{3}{2}}}, \tag{7}$$

$$G = u_1'^2 \frac{\overline{(\partial^2 u_1/\partial t^2)^2}}{[\overline{(\partial u_1/\partial t)^2}]^2} \tag{8}$$

and

$$\lambda^2 = \left[\frac{u_1'^2}{\overline{(\partial u_1/\partial t)^2}}\right] U_1^2. \tag{9}$$

Using the isotropic assumptions, Batchelor & Townsend (1947) further simplified the vorticity equation (3) to the following form:

$$G = \tfrac{30}{7} + \tfrac{1}{2} R_\lambda S, \tag{10}$$

which may be rewritten as (for $S = 0{\cdot}39$ as suggested by Batchelor & Townsend, and neglecting $\frac{30}{7}$ for large R_λ)

$$2G/R_\lambda S = 1{\cdot}0. \tag{11}$$

Based on theoretical considerations, Tatsumi *et al.* (1978) calculated values of S for isotropic turbulence and suggested its upper limit to be 0·65 (lower limit being 0·3). A

value of S higher than 0·39 would further decrease the importance of the first term on the right-hand side of equation (10) and thus provide additional justification for the assumptions of Batchelor & Townsend (1947) in deriving equation (11).

Taylor (1938) indicated that for large Reynolds numbers the vorticity budget (equation 1) may be approximated by

$$\overline{\omega_i \omega_j \frac{\partial u_i}{\partial x_j}} = \nu \overline{\frac{\partial \omega_i}{\partial x_j} \frac{\partial \omega_i}{\partial x_j}}. \tag{12}$$

Equation (12) is the same as equation (11) given by Batchelor & Townsend (1947) for isotropic flow in terms of S, G and R_λ parameters. Both these equations imply that the terms on the left-hand side in equation (1) are approximately zero and, consequently, production of vorticity is balanced by viscous effects. Tennekes & Lumley (1972, pp. 89–91) have provided justifications for the derivation of equation (12), on the basis of the estimation of the order of magnitude of each term of the general vorticity equation (equation (3.3.38), Tennekes & Lumley). They have shown that the production and dissipation terms of equation (12) are of the same order, whereas the transfer terms and the remaining production terms are at least an order of magnitude smaller. Therefore, for high-Reynolds-number turbulence, these other terms can be neglected, thus reducing the vorticity balance to equation (12) (Wyngaard & Tennekes 1970).

The fine structure of turbulence that is responsible for the viscous dissipation (ϵ) can be obtained using the well-known simplified expression

$$\epsilon = \nu \overline{\left[\frac{\partial u_i}{\partial x_j} + \frac{\partial u_j}{\partial x_i}\right] \frac{\partial u_i}{\partial x_j}} = \nu \overline{\left(\frac{\partial u_i}{\partial x_j}\right)^2} = 15\nu \overline{\left(\frac{\partial u_1}{\partial x_1}\right)^2} = \frac{15\nu}{U_1^2} \overline{\left(\frac{\partial u_1}{\partial t}\right)^2}. \tag{13}$$

The above equation makes use of the assumptions of local isotropy and Taylor's hypothesis of frozen turbulence. From equation (13), the Kolmogoroff length (η) and time (τ_η) scales (of fine structures) can be obtained using the expressions

$$\eta = (\nu^3/\epsilon)^{\frac{1}{4}}, \tag{14}$$

and

$$\tau_\eta = (\nu/\epsilon)^{\frac{1}{2}}. \tag{15}$$

The relationship between the large-scale and small-scale structures of turbulence can be studied by evaluating the ratios of the length and time scales of these structures. For this purpose, the length (L_ϵ) and time (τ_ϵ) scales of the energy-containing eddies can be computed (Lumley 1970) from

$$L_\epsilon = q^3/3^{\frac{3}{2}}\epsilon, \quad R_{L\epsilon} = qL_\epsilon/3^{\frac{3}{2}}\nu = q^4/9\nu\epsilon \tag{16), (17}$$

and

$$\tau_\epsilon = q^2/2\epsilon, \tag{18}$$

where q^2 is the trace of the Reynolds stress tensor ($q^2 = u_1'^2 + u_2'^2 + u_3'^2$), where u_1, u_2, u_3 are fluctuating velocities in x_1, x_2, x_3 directions respectively, and the prime designates r.m.s. value.

3. Experimental equipment and procedure

3.1. *Wind tunnel and diffuser*

The experiments were conducted in a low-speed open-circuit wind tunnel described previously by Azad & Hummel (1971). Briefly, air was blown through an 89:1 contraction cone and a 74 diameter length of steel pipe (101·6 mm inside diameter) before entering the diffuser.

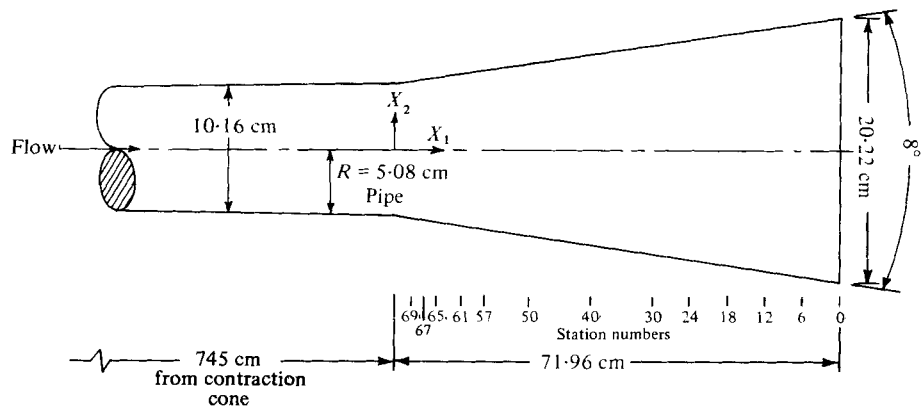

FIGURE 1. Diffuser geometry.

The diffuser (figure 1) was machined from cast aluminium. A machined reinforcement ring (which could be rotated to any angular position) was adapted to the outlet end of the diffuser to support the traversing mechanism which employed a micrometer head graduated in 0·001 mm. The probes were mounted on a 2·5 cm diameter tube entering the diffuser from the downstream end. A taper 22 cm long was fitted between the end of the tube and the probe support to minimize any flow blockage effect upstream of the tube.

Okwuobi & Azad (1973) have shown that the flow in the pipe upstream of the diffuser is fully developed and, by using forward- and reverse-facing pitot tubes, they have also shown that the flow in the diffuser does not separate.

3.2. *Instrumentation*

Mean static pressure along the diffuser wall was measured with a static pressure round tube having an external diameter of 1 mm together with a Betz projection manometer with 0·1 mm of water-scale interval. No corrections were attempted to account for the turbulence.

The derivative of the longitudinal turbulent velocity component ($\partial u_1/\partial t$) was measured with a special DISA 55P01 gold-plated single hot-wire probe (0·625 mm wire length, 2·5 μm wire diameter) set normal to the mean flow. The measurements of q^2 were obtained using a standard DISA 55P51 gold-plated X-probe (1·25 mm wire length, 5 μm wire diameter). The single wire was operated at an overheat ratio of 0·4 and the X-wire at 0·8. The l/d ratio of the wires in each case was 250. The smaller length of the hot wire with relatively large l/d ratio was chosen for improved frequency response of the hot-wire probe used for $\partial u_1/\partial t$ measurements. In practice, the length of the hot wire at best represents a compromise between frequency response and the ratio of signal to noise (Frenkiel & Klebanoff 1975). However, ideally the wire length should be of the order of the Kolmogoroff length, which in the present study varied from 0·06 mm to about 0·14 mm. The wire length was thus in the range of 5 to 10 Kolmogoroff lengths. Therefore, the dissipation estimates (ϵ) used in calculating the length and time scales were corrected using Wyngaard's (1969) analysis for a single wire. However, no such corrections were applied to the measurements of S and G since these were normalized by the quantity $\overline{(\partial u_1/\partial t)^2}$ obtained from

the same probe. Furthermore, the authors are not aware of any satisfactory procedure available in the literature for correcting the factors S and G. DISA 55M01 constant temperature anemometers were used in conjunction with DISA 55D10 linearizers. Also used were a multifunction turbulent processor TM377 and a time differentiator TM-TD-1, details of which have been provided by Arora & Azad (1978*a*).

The hot-wire signal was filtered at 28 kHz before and after each differentiation. For this purpose, three built-in filters of TM377 and a Krohn-Hite 3770 filter were used. To improve the operation of multipliers in TM377 and to decrease the measuring errors, the input signals to the multipliers were amplified considerably but not enough to saturate the corresponding circuit.

Arora & Azad (1978*b*) have shown that even small amounts of dirt depositions on the sensing element can affect its frequency response, thereby giving erroneous results particularly of the moments of differentiated signal. Therefore, special care was taken in the use and operation of the probe for $\partial u_1/\partial t$ measurements.

4. Results and discussion

The parameters used for normalizing the experimental data were the pipe average velocity (U_b) and the pipe radius (R_{pipe}). The radial distribution of data is presented as a function of ξ_2, which is defined as

$$\xi_2 = x_2/R_{\text{pipe}}.$$

4.1. *Preliminary measurements*

Static pressures along the diffuser wall were measured at 42 axial locations for 6 different Reynolds numbers varying from 32 000 to 86 000 based on pipe average velocity and pipe radius. These static pressure measurements were normalized by the average velocity head in the pipe and were found to collapse onto a single curve within the experimental error, thus confirming the existence of Reynolds-number similarity. Based on this finding, a single Reynolds number of 58 000 was chosen for further study.

The longitudinal pressure derivatives in the diffuser were obtained by analytical differentiation of a fourth-order polynomial (best fit to the experimental data) which was then evaluated at the desired axial positions. As shown in figure 2, a pressure gradient difference of more than an order of magnitude existed between the beginning of the diffuser and its exit. In order to study the various regions of pressure gradient, the following axial stations were chosen for detailed study:

69, 67, 65, 61, 57, 50, 40, 30, 24, 18, 12, 6 and 0.

The numbers refer to distance towards the pipe (in cm) from the diffuser exit. It was thought that the study of turbulence vorticity balance at these axial stations would help in understanding the structure of turbulence in the diffuser flow.

The mean axial velocities for the present experiment were similar to the earlier published results of Okwuobi & Azad (1973). Turbulent intensities (u_1', u_2' and u_3') required for the evaluation of q^2 were also similar to that of Okwuobi & Azad (1973). The distribution of the stress tensor was qualitatively similar but quantitatively much in excess of those in pipe flow. Also, the total kinetic energy in the diffuser increased in the downstream direction (Arora & Azad 1978*a*). In the radial direction, the turbulent energy showed a peak which shifted slightly towards the diffuser axis with distance in

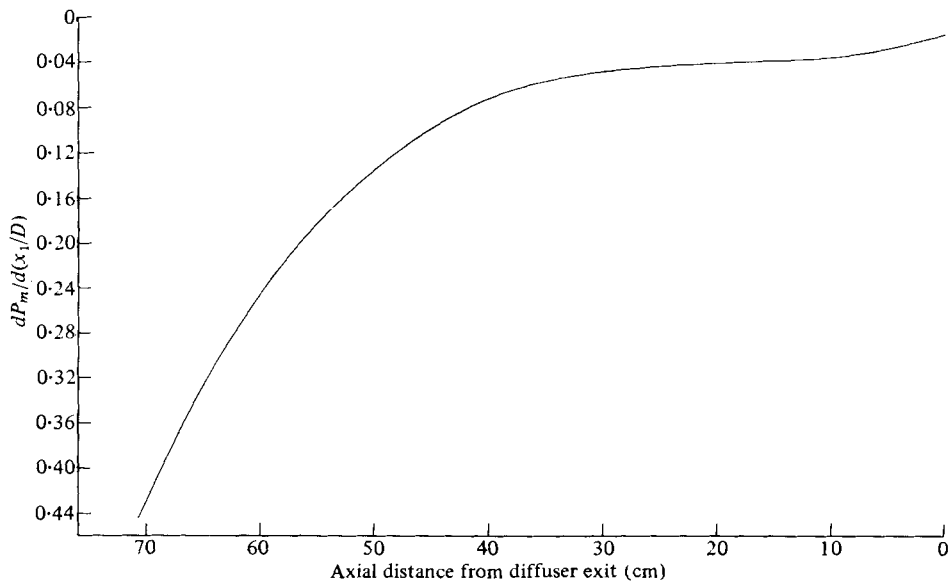

FIGURE 2. Mean static pressure gradient in the diffuser.

the direction of flow. The peak position of q^2 specifies the edge of the wall layer and corresponds to maximum turbulence production (Arora & Azad 1978*a*). In a diffuser, the wall layer (from wall to the maximum q^2) expands in the downstream direction.

4.2. *Length and time scales of flow*

The distribution of the Kolmogoroff's length scale (η) and of Taylor's microscale (λ) are shown in figures 3 and 4 for 7 axial stations, as a function of radial distance ξ_2 from the diffuser axis. The Kolmogoroff's length scale generally decreases in the radial direction (figure 3). However, data at station 50 and further downstream show increases in the values of η close to the wall. The absence of this feature in initial upstream stations is probably due to the lack of data in the wall region. The thickness of the wall layer increases in the downstream direction owing to the expanding flow which allowed measurements of required quantities in this layer without being very close to the wall. Up to station 40 in the downstream direction, values of Kolmogoroff's length scale form essentially a single curve between the diffuser axis and $\xi_2 = 0{\cdot}9$. Further downstream, η values are lower for this radial region and decrease less rapidly with ξ_2. That is, in the axial direction, the magnitude of η away from the wall collapses onto a single curve for large adverse pressure gradients, and decreases in the region of small but constant pressure gradient.

The Taylor's microscale distributions (figure 4) peak in the radial direction at about $\xi_2 = 0{\cdot}4$. From each peak position to the wall, the magnitude of λ decreases monotonically. For a given radial position in the core region, λ increases in the axial direction up to station 40 and then decreases beyond station 30 thus causing crossing over of some of the curves at $\xi_2 = 1{\cdot}0$, as the expanding flow provides larger region to reach the same lower value. However, it is again worth noting that the decrease in λ (like that of η) occurs when most of the pressure recovery has already taken place and the pressure gradient has become more or less constant.

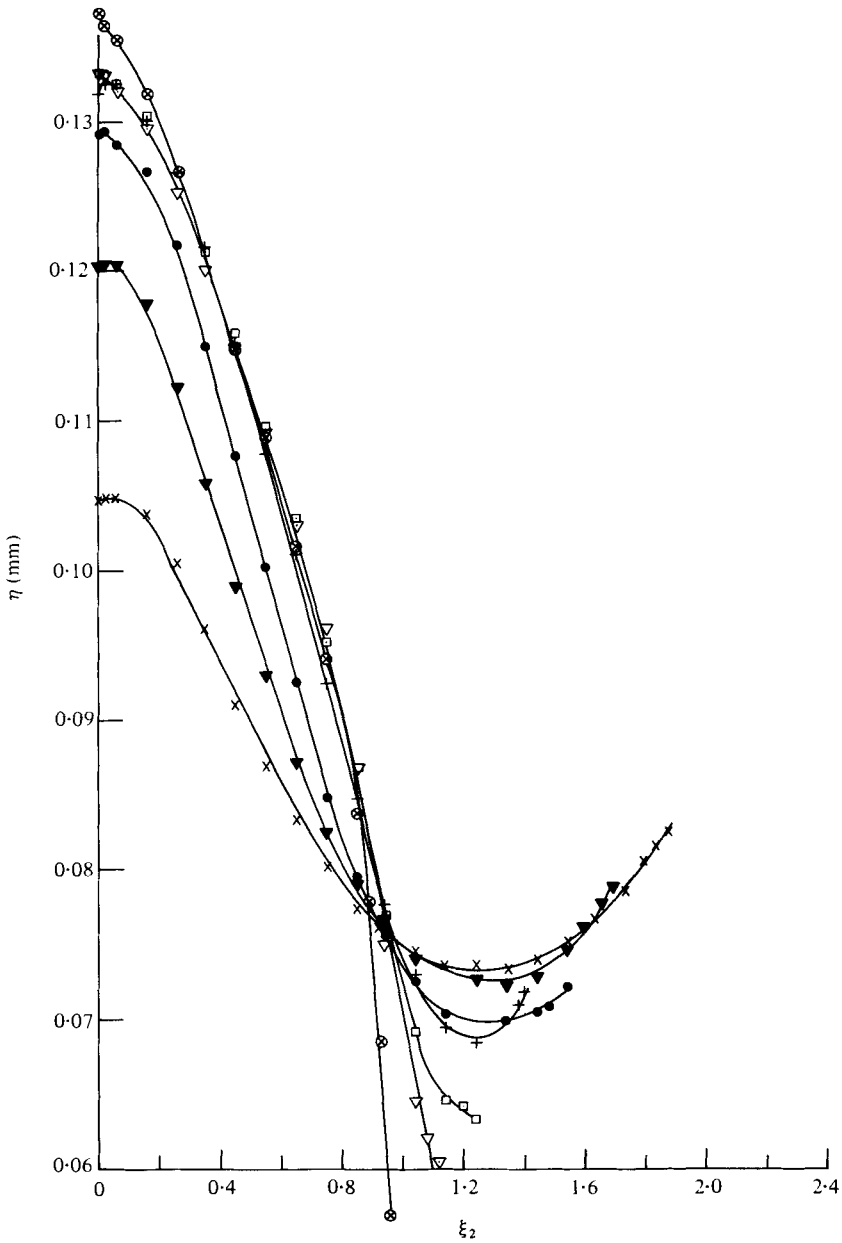

FIGURE 3. Variation of the Kolmogoroff length scale η. Stations (cm): ⊗, 67; ▽, 57; ⊡, 50; +, 40; ●, 30; ▼, 18; ×, 6.

The turbulence Reynolds number R_λ, obtained using λ values [equation (6)], also shows a peak initially appearing at about $\xi_2 = 0{\cdot}80$ which shifts slightly with distance in the downstream direction (figure 5). The magnitude of R_λ generally increases in the direction of flow, thus indicating an increase in turbulence in the flow field.

The Kolmogoroff time scale of the flow (τ_η) is shown in figure 6 for only 3 axial

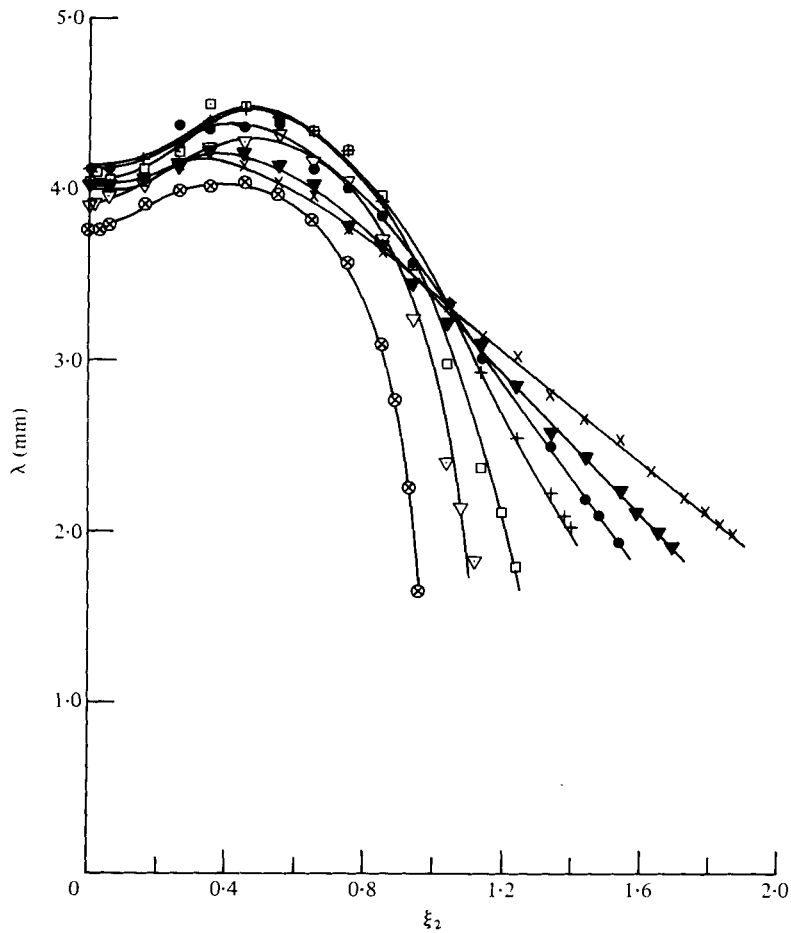

FIGURE 4. Distribution of the Taylor's microscale λ. See figure 3 for the symbols.

stations. These stations represent the main distinct regions of the pressure gradient curves of figure 2. The time scale decreases with increasing radial distance from the axis but increases again near the wall as is indicated by the two curves for stations towards the exit.

In an attempt to understand the interrelationship between the larger and smaller structures of turbulence, the ratio of the two length and time scales were studied. The length and time scales of the energy-containing eddies were obtained using equations (16) and (18). These ratios are shown in figures 7 and 8. Both these ratios have a peak at about $\xi \approx 0{\cdot}75$ in the entry region of the diffuser which shifts towards the diffuser axis in the downstream direction. From the peak position towards the wall, these ratios decrease linearly with radial distance. In the axial direction, the magnitudes of the ratios increase in the direction of the flow. Also, this magnitude at the exit is about twice that at entry for both the ratios. Large values of these ratios, as found in the present study, indicate that the dissipating eddies are independent of the large-energy-extracting eddies. This is in agreement with the conclusions of Tatsumi *et al.* (1978). The characteristic Reynolds number [equation (17)] for the diffuser flow had a similar

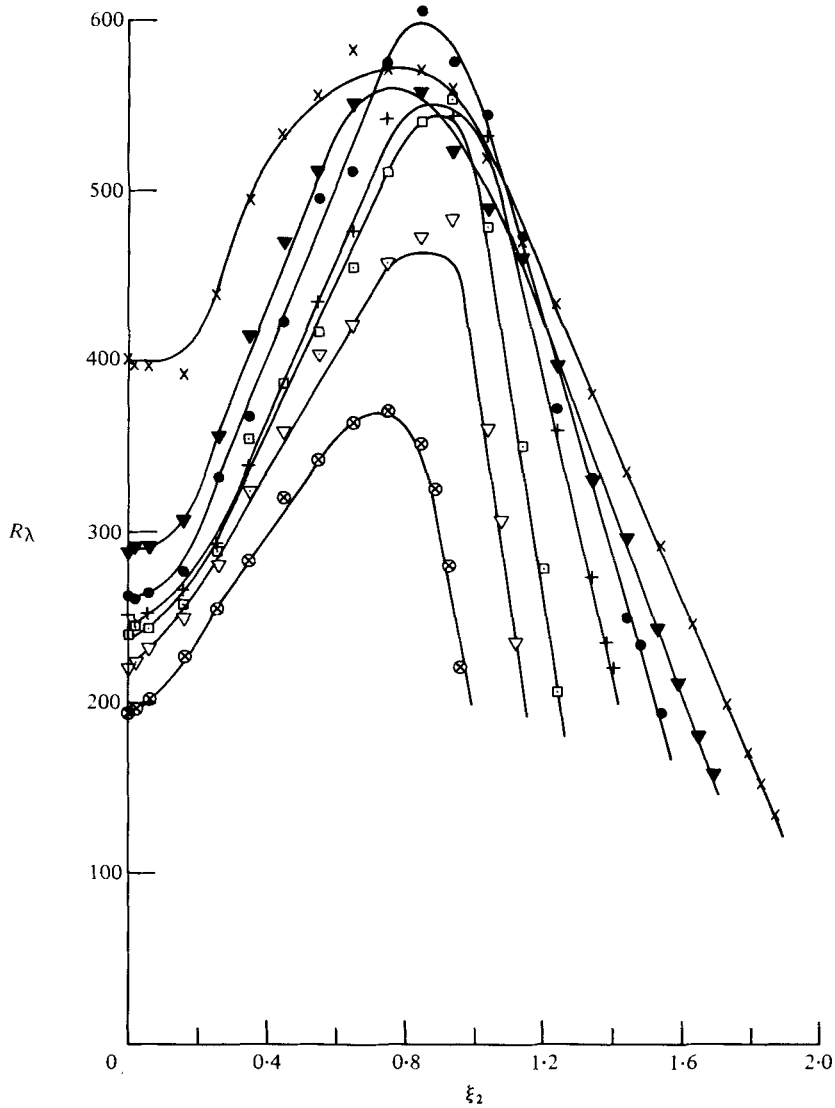

FIGURE 5. The turbulence Reynolds number R_λ in the diffuser. See figure 3 for the symbols.

variation as indicated by the ratios of length scales (figure 7). However, the magnitude of the $R_{L\epsilon}$ was approximately an order of magnitude higher than the ratios of the length scales.

4.3. *Skewness (S) of* $\partial u_1/\partial t$

Measurements of S (equation 7) for 7 different axial stations are shown in figure 9. Curves for the other 6 stations had similar distribution. As figure 9 indicates, values of S range between 0·38 and 0·5 from the diffuser axis to (approximately) the pipe radius ($\xi_2 = 1{\cdot}0$), the latter corresponding approximately with the maximum of u_1' fluctuations. A similar range for the values of S was reported by Batchelor & Townsend (1947) for a grid-generated isotropic turbulence. They suggested that S is essentially constant and has an average value of 0·39. A value of 0·37 was reported by Kuo & Corrsin (1971)

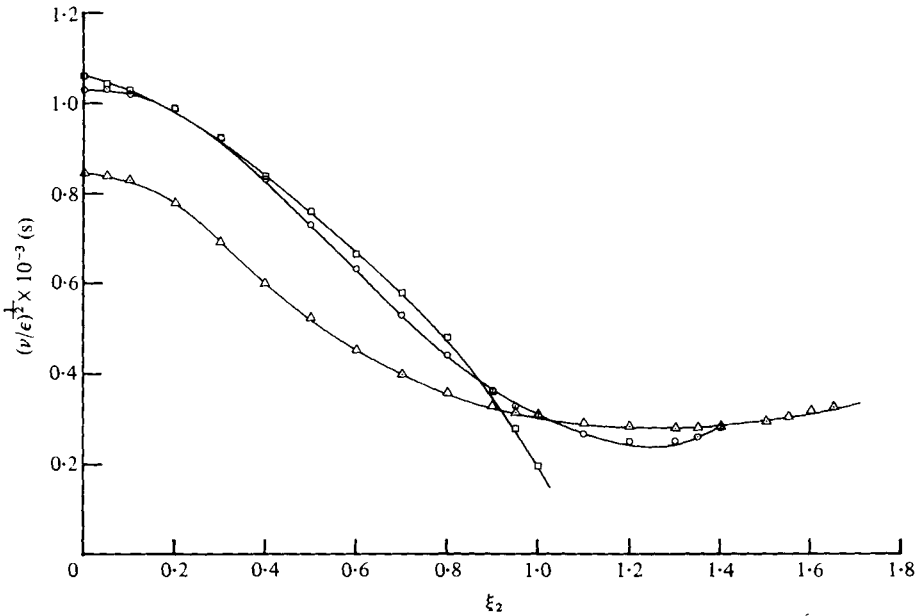

FIGURE 6. Distribution of the Kolmogoroff time scale τ_η. Stations (cm): △, 18; ○, 40; □, 61.

and a value of 0·44 was estimated by Kolmogoroff (Batchelor 1947). Betchov (1956) reported it to vary between 0·4 and 0·5, whereas Saffman (1963) suggested its range to be from 0·3 to 0·5. A value of 0·42 was reported by Wyngaard & Tennekes (1970) for a mixing layer. Recently Tatsumi *et al.* (1978) obtained values of S on the basis of theoretical considerations and reported its limits to be from 0·3 to 0·65 for isotropic turbulence. The present results of S from axis to $\xi_2 \approx 1{\cdot}0$ compare favourably with these values. In the wall region (between the wall and the point of maximum u_1' fluctuations), however, values of S increase with distance towards the wall. Near the diffuser exit, the magnitude of S near the wall reaches as high as 1·0. Since the data very close to the wall were not obtained, its behaviour further towards the wall for the diffuser is not known. In the entry region, the limited data on S obtained in the relatively thin wall region were not as high as 1·0.

The increasing nature of S near the wall has also been reported by Ueda & Hinze (1975) in a flat-plate boundary layer, and by Ueda & Mizushina (1977) and by Elena (1977) in a fully-developed pipe flow. Their results indicate that, very close to the wall, S increases with increasing distance from the wall and reaches its maximum value in the region $10 < y^+ < 20$. Thereafter, it starts to decrease with increasing y^+ (decreasing ξ_2) and reaches a constant value of 0·38 at $y^+ \geqslant 100$. The present results are in agreement with these previously published results in wall-bounded flows, thereby indicating that the fine structure of turbulence is similar. Thus, there is a possibility that, even in the diffuser, S would decrease after reaching its maximum value. However, a notable difference is that, in the boundary layer and the pipe, S attains its maximum value approximately at the point where turbulent production is maximum, whereas it remains constant up to the point of maximum production in the diffuser.

Since the distribution and the magnitude of S in the diffuser, except in the wall layer,

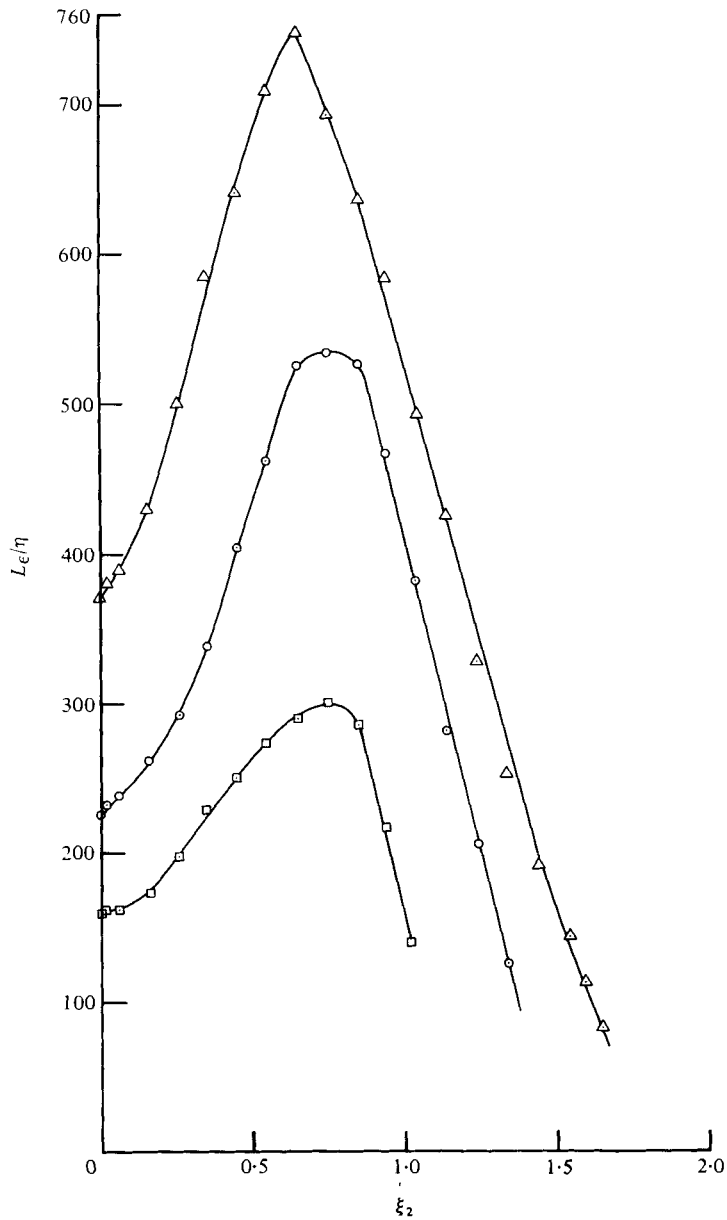

FIGURE 7. Ratio of the characteristic length scale to that of the Kolmogoroff scale L_ϵ/η. See figure 6 for the symbols.

is similar to that for an isotropic flow, it can be argued that the assumption of local isotropy in the diffuser away from the wall is justified. With the same argument, it can be said that the increasing values of S near the wall indicate the increasing degree of anisotropy. Arora & Azad (1978*a*) have shown that the ratio of u_1'/u_2' in the diffuser increases towards the wall, which is a consequence of increase in degree of anisotropy. This is also evident from the flatness factor of $\partial u_1/\partial t$ (figure 10) which is similar to that of boundary layer reported by Frenkiel & Klebanoff (1975). They pointed out that the

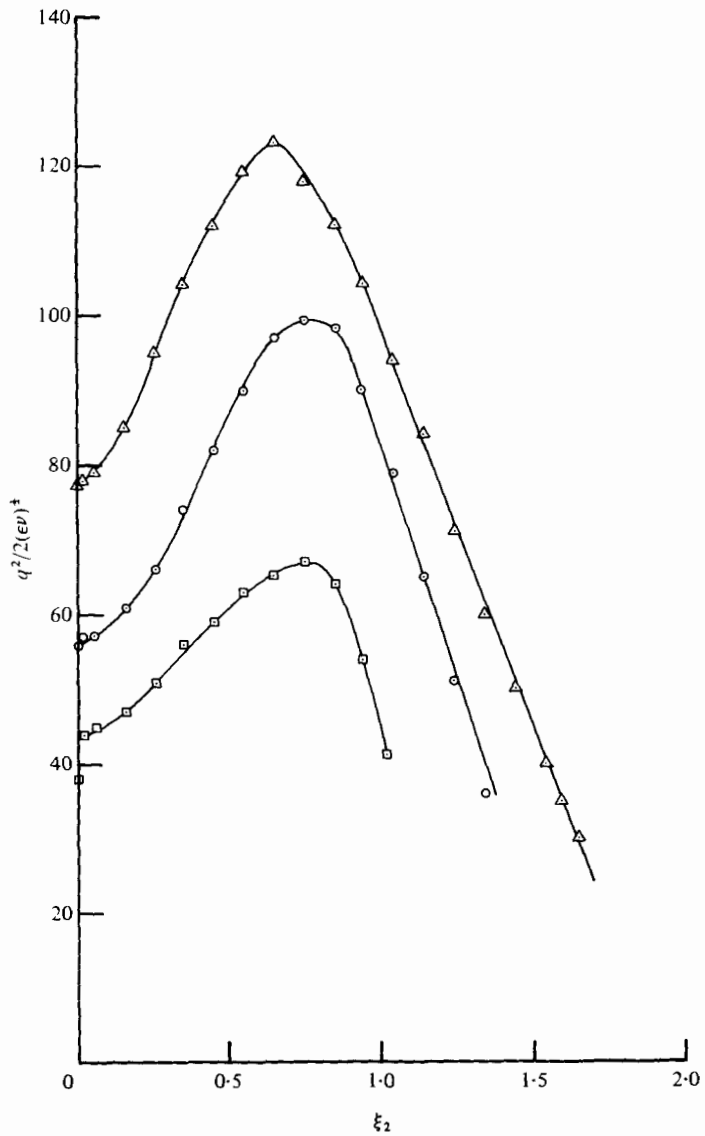

FIGURE 8. Ratio of the characteristic time scale of the flow to that of the dissipative time scale τ_c/τ_η. See figure 6 for the symbols.

assumption of local isotropy is only valid where the flatness factor of $\partial u_1/\partial t$ is constant. Present results indicate that the flatness factor and the skewness of $\partial u_1/\partial t$ are both constant in the region from diffuser axis to about $\xi_2 \approx 1{\cdot}0$. Also, in the boundary layer, Klebanoff (1978, private communication) found S to be constant in the region of constant $F(\partial u_1/\partial t)$. Further towards the wall, the skewness and flatness factor of $\partial u_1/\partial t$ increase with the increasing distance towards the wall. However, their respective variations are such that $S\alpha F^{\frac{1}{2}}(\partial u_1/\partial t)$ (which satisfies the inequality

$$F^{\frac{1}{2}}(\partial u_1/\partial t) \geqslant \tfrac{1}{2}\sqrt{21}$$

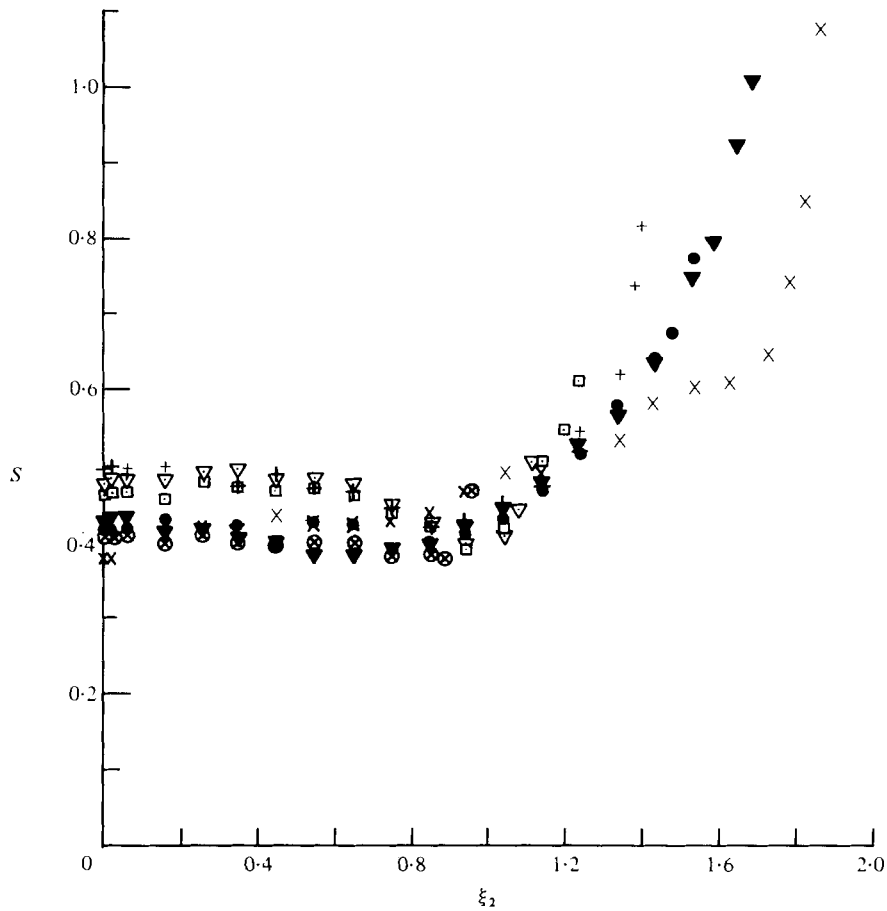

FIGURE 9. Variation of the skewness of $\partial u_1/\partial t$ at axial station 7. See figure 3 for the symbols.

proposed by Betchov, 1956), thus indicating the intermittency of the fine-scale structure in the wall layer. This is in agreement with the results of an intermittency factor of $\partial u_1/\partial t$ and the maximum flatness factor of filtered u_1 at station 30 for the same diffuser reported by Azad & Hummel (1979). Both of these quantities were reported to be almost constant from the diffuser axis to about $\xi_2 \approx 1{\cdot}0$, where the intermittency factor was unity and the maximum flatness factor of filtered u_1 was about 22. In the wall layer, however, the maximum flatness factor increased and the intermittency factor decreased with the distance, thus indicating the finer structure to be spotty and intermittent.

Batchelor & Townsend (1947) reported that the measurements of S in their flow were independent of the turbulence Reynolds number R_λ. The values of R_λ in their flow varied from 20 to 60. For the region where S remained approximately constant (within the range 0·37 to 0·5) in the diffuser, the turbulence Reynolds number R_λ varied from 200 to 600 (figure 11), which is an order of magnitude higher than that of the grid turbulence reported by Batchelor & Townsend (1947). The values of S obtained in the wall region of the diffuser deviated from this range and are not shown in figure 11.

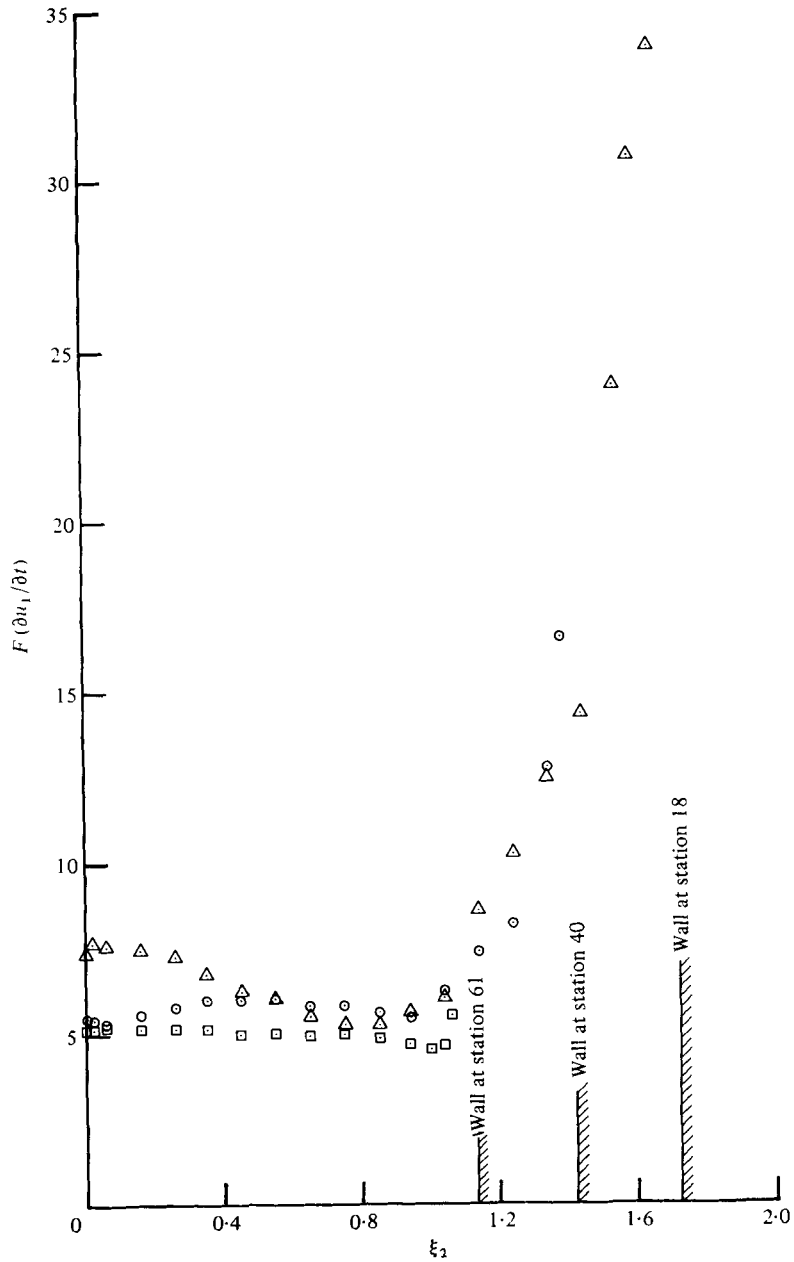

FIGURE 10. Flatness factor of $\partial u_1/\partial t$. See figure 6 for the symbols.

4.4. *Second derivative of* u_1 (G)

Measurements of G which represent the decay of vorticity in the flow field due to viscosity were generally found to increase in magnitude in the axial direction. In the radial direction, it also shows a rising trend near the diffuser wall. The increasing values of G indicate that the effect of viscosity in smoothing out turbulent fluctuations is also increasing. However, in the vorticity equation (3), parameter G appears as G/R_λ.

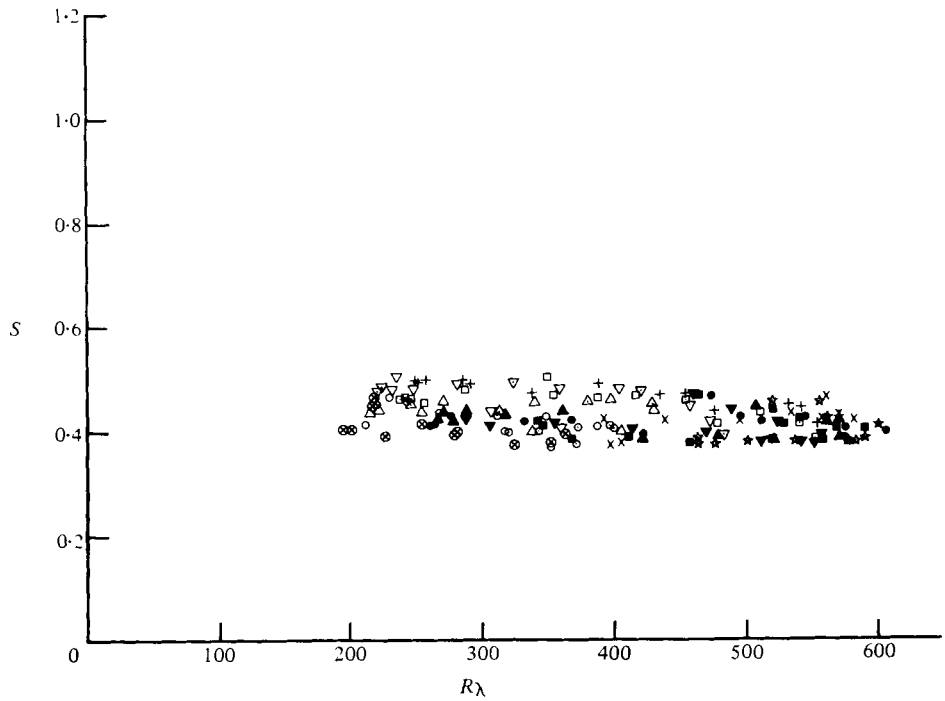

FIGURE 11. Distribution of S as a function of R_λ. Stations (cm): ⊗, 67; ○, 65; △, 61; ▽, 57; ⊡, 50; +, 40; ●, 30; ▲, 24; ▼, 18; ■, 12; ×, 6; ★, 0.

Since G and R_λ both increase in the downstream axial direction, their ratio (figure 12, owing to similarity, data for 7 stations only are presented) was found to be independent of the axial position, thus indicating the linear dependence of G on R_λ. This also shows that the viscosity effects adjust themselves according to the Reynolds number and are always maintained at a finite level in the flow field. In the radial direction, the ratio G/R_λ is constant from the diffuser axis to $\xi_2 \approx 1{\cdot}0$ and increases sharply further towards the wall. This behaviour is similar to that of S (figure 9) and indicates a close relationship between the production of vorticity and its decay in the flow field.

4.5. *Vorticity balance*

To check the applicability of equation (10) for the flow under investigation, values of G (excluding the wall layer) were plotted as a function of R_λ (figure 13). The solid line represents equation (10) with $S = 0{\cdot}39$ as suggested by Batchelor & Townsend for isotropic flow. Agreement between the grid turbulence data ($20 \leqslant R_\lambda \leqslant 60$) and the diffuser data ($200 \leqslant R_\lambda \leqslant 600$) is excellent. This shows that Batchelor & Townsend's (1947) analysis of isotropic turbulence is equally valid for the present complex flow for an order-of-magnitude higher R_λ, thus justifying the extension of the isotropic ideas to the core region of the diffuser flow.

The approximate isotropic vorticity budget (11) was also evaluated for the diffuser flow. As figure 14 indicates, equation (11) also holds approximately true in the core region of the diffuser where S and G/R_λ were both constant. These results in the core region, though, show some variation, but generally do confirm the applicability of (11)

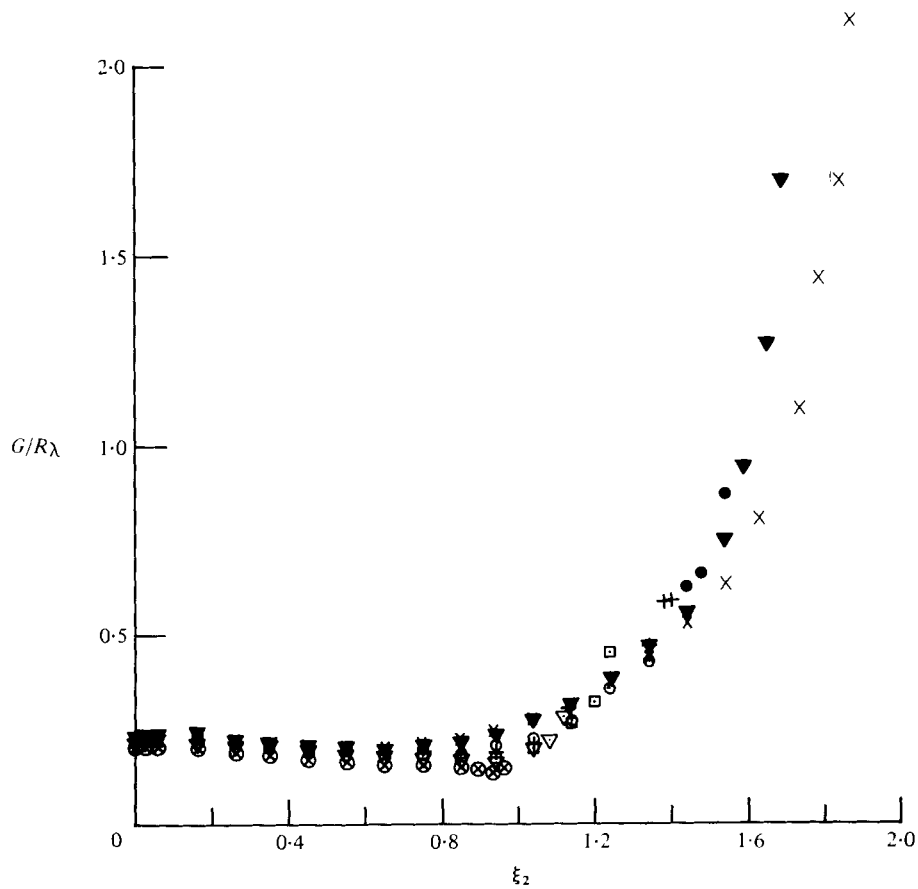

FIGURE 12. Distribution of G/R_λ in the diffuser. See figure 3 for the symbols.

and, in turn, justify its extension to the diffuser flow. Since the quantity $2G/R_\lambda S$ represents a ratio of decay to production of vorticity, its magnitude near unity implies that the rates of production and dissipation are essentially equal. This suggests that there is a dynamical similarity at all axial stations of those aspects of the turbulence which control the vorticity balance. However, in the wall layer, the plot of $2G/R_\lambda S$ increases with the increasing radial distance towards the wall (figure 15). This indicates that the effect of viscosity is greater and exceeds the effect of vortex extension in the wall layer, which contradicts (12). This imbalance in the magnitude of production and dissipation in the wall layer would increase the significance of transfer terms in the general vorticity balance equation. These terms, thus, could no longer be considered negligible and the isotropic vorticity balance equation would not represent the true nature of the fine structure in the wall layer of the diffuser. This supports the Kolmogoroff's (1941) hypothesis of local isotropy, which 'is realized on domains not lying near the boundary of the flow or its other singularities'.

Thus the results confirm that, even in shear flows, there exists a region which has certain similarities to that of an isotropic flow. The presence of the wall and the ensuing complexities prohibit the extension of these isotropic ideas to the wall layer.

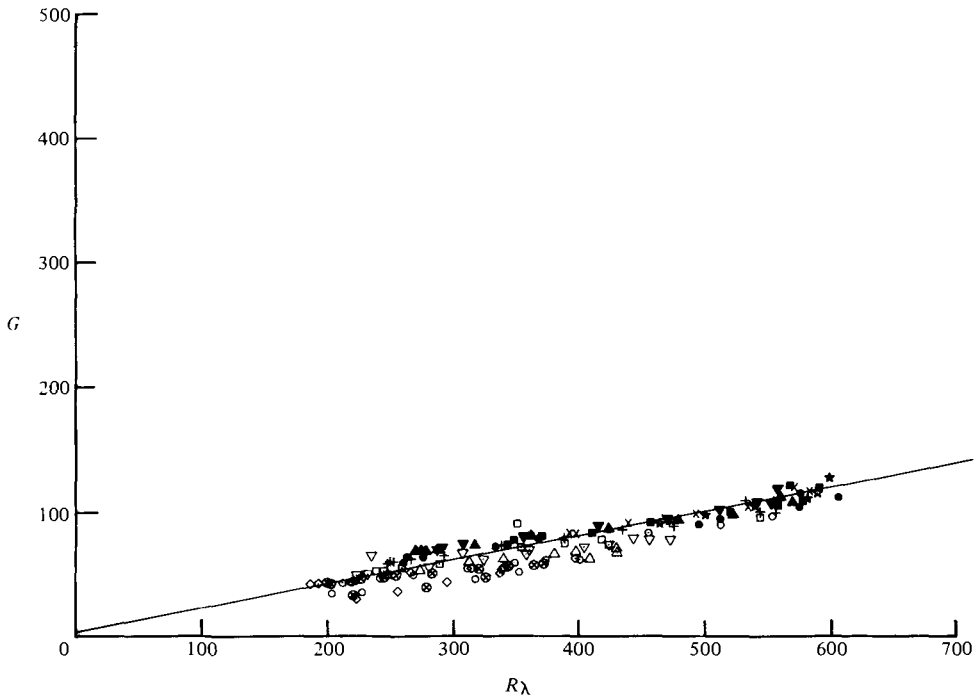

FIGURE 13. Variation of G as a function of R_λ. ◇, station at 69 cm. See figure 11 for the other symbols.

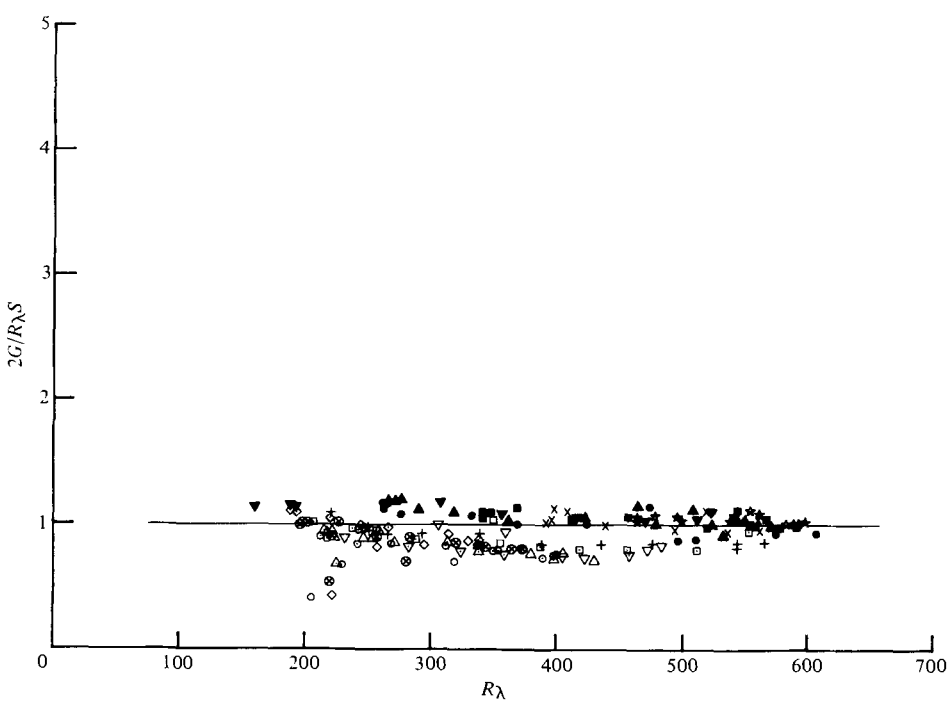

FIGURE 14. Ratio of the dissipation and production of vorticity as a function of R_λ. See figures 11 and 13 for the symbols.

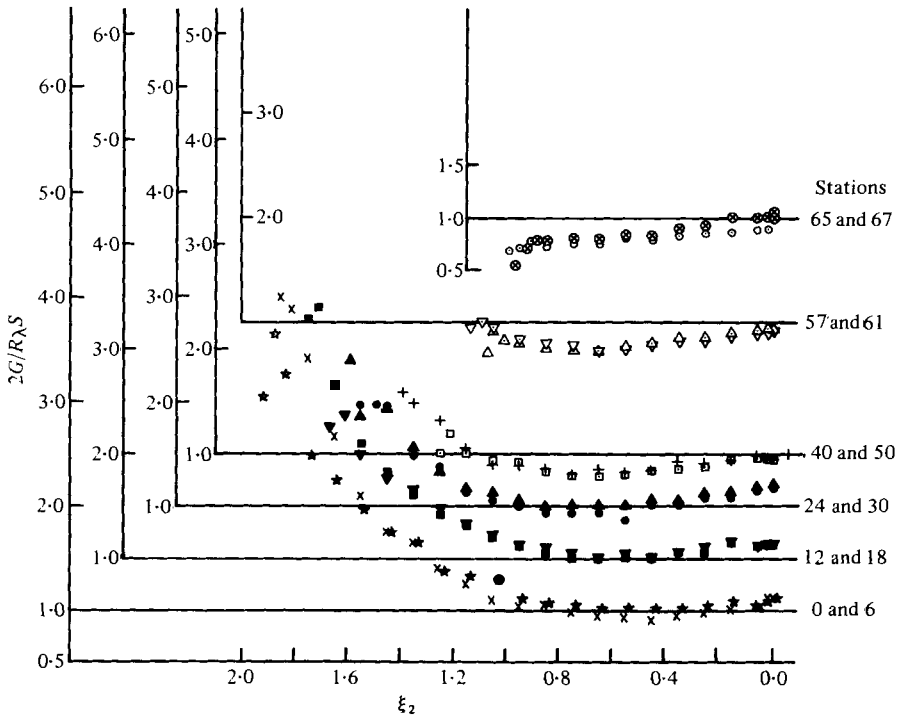

FIGURE 15. Ratio of the dissipation and production of vorticity. See figure 11 for the symbols.

5. Conclusions

Detailed experimental measurements of the first and second derivatives of the u_1 signal were made in the diffuser. Since these measurements put more emphasis on the higher frequency components and thus the fine structure of turbulence, their study was undertaken to investigate the applicability of the isotropic theory of vorticity production and its eventual decay in the diffuser.

The results show that Batchelor & Townsend's (1947) analysis for isotropic turbulent vorticity balance is equally valid for an order-of-magnitude higher R_λ in the diffuser flow except in the wall layer. In the core region, where this analysis is applicable, the ratio of the rates of production and dissipation of ω'^2 was constant, and the vorticity balance was essentially the same at all axial stations.

In the wall region, however, vorticity parameters S and G do not follow isotropic patterns, but the behaviour of S is similar to other wall-bounded flows. However, its maximum does not coincide to the point of maximum u_1' fluctuations as in fully-developed pipe flow, but rather is attained closer to the wall. This provides a larger region in the diffuser where the distribution of S is constant as compared to pipe flow.

On the basis of the present findings, it is concluded that, even in a shear flow subjected to adverse pressure gradient, the isotropic theory of vorticity can be applied to a region far removed from the wall.

The authors would like to thank Dr J. Hunt and the referees for their corrections and suggestions. This work was supported by the Natural Sciences and Engineering Research Council of Canada.

REFERENCES

ARORA, S. C. & AZAD, R. S. 1978*a* *Univ. Manitoba, Winnipeg, Canada, Dept. Mech. Engng, Rep.* no. ER25.27.

ARORA, S. C. & AZAD, R. S. 1978*b* *Univ. Manitoba, Winnipeg, Canada, Dept. Mech. Engng, Rep.* no. ER25.28.

AZAD, R. S. & HUMMEL, R. H. 1971 *Can. J. Phys.* **49**, 2917.

AZAD, R. S. & HUMMEL, R. H. 1979 *A.I.A.A. J.* **17**, 884.

BATCHELOR, G. K. 1947 *Proc. Camb. phil. Soc.* **43**, 533.

BATCHELOR, G. K. & TOWNSEND, A. A. 1947 *Proc. Roy. Soc.* A **191**, 534.

BETCHOV, R. 1956 *J. Fluid Mech.* **1**, 497.

CORRSIN, S. & KISTLER, A. L. 1955 *N.A.C.A. Rep.* 1244.

ELENA, M. 1977 *Int. J. Heat & Mass Transfer* **20**, 935.

FRENKIEL, F. N. & KLEBANOFF, P. S. 1975 *Boundary-Layer Meteorol.* **8**, 173.

KOLMOGOROFF, A. N. 1941 *Comptes rendus de l'Académie des sciences de l'U.R.S.S.* **30**, 301. (English translation: 1961 *Turbulence, Classical Papers on Statistical Theory* (ed. S. K. Friedlander & L. Topper), paper 7, p. 151. Interscience.)

KUO, A. Y. S. & CORRSIN, S. 1971 *J. Fluid Mech.* **50**, 285.

LUMLEY, J. L. 1970 *J. Fluid Mech.* **41**, 413.

OKWUOBI, P. A. C. & AZAD, R. S. 1973 *J. Fluid Mech.* **57**, 603.

SAFFMAN, P. G. 1963 *J. Fluid Mech.* **16**, 545.

SOVRAN, G. & KLOMP, E. D. 1967 *Gen. Motors Symp. on Internal Flow.* Elsevier.

TATSUMI, T., KIDA, S. & MIZUSHIMA, J. 1978 *J. Fluid Mech.* **85**, 97.

TAYLOR, G. I. 1935 *Proc. Roy. Soc.* A **151**, 421.

TAYLOR, G. I. 1938 *Proc. Roy. Soc.* A **164**, 15.

TENNEKES, H. & LUMLEY, J. L. 1972 *A First Course in Turbulence.* M.I.T. Press.

UEDA, H. & HINZE, J. O. 1975 *J. Fluid Mech.* **67**, 125.

UEDA, H. & MIZUSHINA, T. 1977 *5th Biennial Symp. on Turbulence, University of Missouri-Rolla.*

WYNGAARD, J. C. 1969 *J. Phys.* E *Sci. Instr.* **2**, 983.

WYNGAARD, J. C. & TENNEKES, H. 1970 *Phys. Fluids* **13**, 1962.